

# Role of Ion–Dipole Interactions in Nucleation of Gamma Poly(vinylidene fluoride) in the Presence of Graphene Oxide during Melt Crystallization

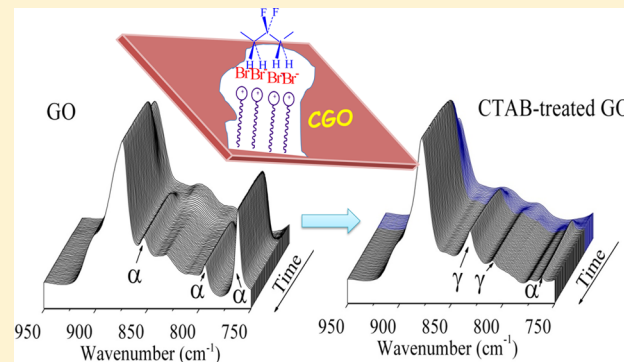
Yue Li,<sup>†</sup> Jia-Zhuang Xu,<sup>†</sup> Lei Zhu,<sup>‡</sup> Gan-Ji Zhong,<sup>\*,†</sup> and Zhong-Ming Li<sup>\*,†</sup>

<sup>†</sup>College of Polymer Science and Engineering, State Key Laboratory of Polymer Materials Engineering, Sichuan University, Chengdu, 610065, Sichuan, People's Republic of China

<sup>‡</sup>Department of Macromolecular Science and Engineering, Case Western Reserve University, Cleveland, Ohio 44106-7202, United States

## Supporting Information

**ABSTRACT:** The crystallization behavior and crystalline structure of poly(vinylidene fluoride) (PVDF) in the presence of graphene oxide (GO) platelets were investigated using time-resolved Fourier transformation infrared spectroscopy (FTIR), wide-angle X-ray diffraction (WAXD), as well as differential scanning calorimetry (DSC). It is shown that GO platelets induce the formation of  $\gamma$  phase when crystallizing from solution, but only  $\alpha$  phase forms from melt crystallization. The crystallization kinetics of  $\alpha$  phase is promoted due to heterogeneous nucleation ability of GO, which is probably originated from a weak  $\pi$ -dipole interaction between GO and PVDF. Intriguingly, after introduction of strong ion–dipole interactions between GO and PVDF by addition of an ionic surfactant (cetyltrimethylammonium bromide, CTAB), a significant amount of  $\gamma$  crystals are obtained during isothermal melt crystallization. Time-resolved FTIR results further provide a detailed evolution of the  $\gamma$  phase formation, and there are two distinct stages during the melt crystallization in the PVDF/GO composites in the presence of CTAB, i.e., a simultaneous growth of  $\gamma$  and  $\alpha$  phases in the first stage, and a solid  $\alpha$  to  $\gamma$  transition in the second stage. These results may provide a facile routine to manipulate the crystalline structure in PVDF/GO composites, and thus to gain desirable properties.



## 1. INTRODUCTION

Poly(vinylidene fluoride) (PVDF) can crystallize into at least four polymorphs ( $\alpha$ ,  $\beta$ ,  $\gamma$ , and  $\delta$ ), which results in different ferroelectric properties.<sup>1–3</sup> The  $\alpha$  phase, which is the most kinetically favored, has the trans-gauche conformation (TGTG').<sup>1</sup> The orthorhombic  $\beta$  phase has the all trans-conformation (TTTT) with two chains in a unit cell. The  $\gamma$  phase has a gauche conformation (G) every fourth repeating unit (T<sub>3</sub>GT<sub>3</sub>G').<sup>2</sup> In the  $\alpha$  and  $\gamma$  phases, the crystal structure can adopt either orthorhombic or monoclinic modification, depending on whether the chains are statistically packed or not.<sup>4</sup> Compared with the  $\alpha$  phase, the polar  $\beta$  and  $\gamma$  phases have attracted much attention due to their unique physical properties and potential applications. For example, the polar  $\beta$  and  $\gamma$  phases give rise to pyroelectricity,<sup>5</sup> piezoelectricity,<sup>6</sup> and ferroelectricity.<sup>7</sup> Meanwhile,  $\gamma$  phase increases transparency, which makes it appropriate for optical devices.<sup>8</sup>

The  $\gamma$  phase (and/or  $\beta$  phase) can be induced by a heterogeneous phase, which depends on the local field–dipole interactions including ion–dipole, dipole–dipole, hydrogen bond–dipole, and even external electric field–dipole interactions. These local field–dipole interactions usually exist in the

case of polar interfaces of multiphase systems, which can be either inorganic<sup>9–14</sup> or polymeric.<sup>15–18</sup> Inorganic polar interfaces include those from inorganic salts [e.g., (001) surfaces in KBr and NaCl],<sup>9,10</sup> charged nanoplatelets (e.g., mica and layered silicates),<sup>11,12</sup> or even electron-rich carbon nanotubes.<sup>13,14</sup> Polymeric polar interfaces could exist in PVDF blends, such as PVDF/poly(vinyl chloride)<sup>15</sup> and PVDF/nylon 11 blends.<sup>16,17</sup> Our previous studies on the polar phase formed in as-electrospun PVDF/polyarylonitrile (PAN) blend fibers also show that the dipolar interaction between PAN and PVDF plays an important role in the polar phase formation in addition to the mechanical stretching effect. Even after removal of the mechanical stretching during the melt-recrystallization process, a significant amount of ferroelectric phase persists.<sup>18</sup>

Graphene is a two-dimensional (2D) carbon nanofiller or planar sheet of sp<sup>2</sup> bonded carbon atoms with high surface area and aspect ratio,<sup>19</sup> and its PVDF composites have attracted increasing interest in recent years, because they show many

Received: September 4, 2012

Revised: November 18, 2012

Published: November 29, 2012

promising properties, such as mechanical, barrier, thermal, electric, and electromagnetic interference shielding properties.<sup>20–22</sup> Although the local electric field-dipole interactions have not been identified clearly, formation of polar phases was reported in PVDF/graphene systems. For example, Nandi et al. obtained the pure  $\beta$  phase of PVDF by addition of a poly(methyl methacrylate) (PMMA)-grafted-graphene oxide (GO).<sup>23</sup> Qaiss et al. observed pure  $\beta$  phase by addition of pristine GO,<sup>24</sup> and Zhang et al. reported that graphite nanosheet could induce the  $\beta$  and  $\gamma$  phases while reducing the amount of  $\alpha$  phase.<sup>25</sup> However, these studies are focused on the crystallization from PVDF solution, and it is hard to rule out the effect of the interactions between solvents and PVDF.<sup>26,27</sup> To the best of our knowledge, a systematic evaluation of the influence of GO–PVDF interaction on polymorphism of PVDF during melt crystallization is not reported, although most of the shaping in the manufacture of PVDF objects is carried out in the melt state.

In the present work, melt-crystallization of PVDF in PVDF/GO platelet composites has been investigated by using time-resolved Fourier transformation infrared spectroscopy (FTIR) and wide-angle X-ray diffraction (WAXD). It is shown that the kinetics of crystallization of  $\alpha$  phase is promoted due to the heterogeneous nucleation ability of GO; however, GO does not have the ability to induce polar phase of PVDF, inferring that only weak interactions may exist between PVDF and GO. Subsequently, we explored the possibility of complete polar phase nucleation by introduction of a strong ion-dipole interaction in PVDF/GO platelet composites. By addition of an ionic surfactant (cetyltrimethyl ammonium bromide, CTAB), nearly pure  $\gamma$  crystals were successfully obtained due to these ion-dipole interactions during melt crystallization for the first time. In addition, time-resolved FTIR shows that CTAB-treated GO (CGO) can induce the nucleation and growth of  $\gamma$  phase preferentially in the early stage, and enhance  $\alpha$ - $\gamma$  solid state transformation in the later stage.

## 2. EXPERIMENTAL SECTION

**2.1. Materials.** The PVDF (FR903) used in this study was purchased from 3F Co, Shanghai, China (MFR= 2 g/10 min). CTAB and *N,N*-dimethyl formamide (DMF) were purchased from Chengdu Kelong Chemical Reagent Factory (China). They were used without further purification.

**2.2. Sample Preparation. Preparation and Treatment of GO Platelets.** GO platelets were prepared from expanded graphites by oxidizing with KMnO<sub>4</sub>/NaNO<sub>3</sub> mixture in concentrated H<sub>2</sub>SO<sub>4</sub> medium using the modified Hummers method as we described elsewhere.<sup>28</sup> The surface treatment of GO platelets by ionic surfactant was carried out as follows. First, a well-dispersed GO platelet/DMF suspension with a concentration 0.5 mg/mL was prepared by ultrasonication for approximately 4 h in DMF. Then, CTAB (4 mg/10 mL) was added into the GO/DMF suspension. After mechanical stirring for 1 day, the mixture was filtered, and subsequently a significant amount of deionized water was used to help remove the free CTAB. After this process, the mixture was dried in a vacuum oven at 60 °C for 48h, which was called CGO in the context. The concentration of CTAB in the CGO is about 25 wt % (see Figure S1, Supporting Information).

**Preparation of PVDF/GO (or CGO) Platelet Composites.** For preparation of PVDF/GO platelet composites, the PVDF solution was first prepared by dissolving PVDF pellets in DMF (5 wt %) with stirring for 3 h at 60 °C. Afterward, a certain

amount of GO/DMF suspension prepared previously was added into the PVDF solution to achieve the designed weight ratio of GO to PVDF in the range of 0.1–1 wt %. The mixtures were stirred at room temperature for another 2 h in order to achieve a homogeneous system. The PVDF/CGO nanocomposites were prepared by using the same procedure; the only difference was that the dispersion of CGO only cost 2 h since the surfactant is favorable for dispersion. The dispersion of GO or (CGO) in the nanocomposites is fairly good, and most GO (or CGO) was well exfoliated (see Figure S2). To investigate the crystallization of PVDF from solution in the presence of GO, the mixtures of PVDF/GO/DMF were poured into Petri dishes, and then the Petri dishes were moved to an oven for solution crystallization at 120 °C for 2h. The thin films thus obtained were used for investigation of solution (or melt) crystallization in the presence of GO platelets (or CGO). Neat PVDF sample was prepared using the same procedure as the nanocomposites.

**2.3. Characterizations. FTIR.** The crystalline structure and the conformation transformation during melt crystallization were analyzed by time-resolved FTIR (Nicolet 6700, Thermal Scientific, USA). The FTIR was assembled with a parallel-plate cell as a hot stage (the accuracy of  $\pm 1$  °C). The thin film of PVDF/GO (CGO) composites ( $\sim 20$   $\mu$ m) was sandwiched between two ZnSe plates in order to fit into the transmission mold. The spectra over the wavenumber range of 650–4000  $\text{cm}^{-1}$  were obtained by averaging 16 scans at a resolution of 2  $\text{cm}^{-1}$  with 1 min intervals. For the melt crystallization, the samples were kept at 210 °C for 10 min to erase any thermal history and then cooled rapidly to a preset crystallization temperature  $T_c$  (160 °C in less than 4 min); when the temperature reached 160 °C, data collection was started until crystallization was complete. The baseline of each spectrum was linearly corrected according to the same standard. For investigation of melting behavior, the heating rate was 1 °C/min. Data collection was performed from 140 to 200 °C after isothermal crystallization.

**WAXD.** The WAXD measurements were conducted under room temperature at beamline 15U of the Shanghai Synchrotron Radiation Facility, China. The wavelength of monochromated X-ray was 0.124 nm, and the beam size was ca. 400  $\mu$ m. 2D WAXD patterns were collected with an X-ray CCD detector (Model Mar345). An aluminum oxide (Al<sub>2</sub>O<sub>3</sub>) standard was used to calibrate the scattering angle, and the background of air scattering was subtracted. The distance from the sample to detector was 185 mm. Linear WAXD profiles were obtained from circularly integrated intensities of the 2D WAXD patterns.

**Differential Scanning Calorimeter (DSC).** A DSC (TA Q200) was used to study the melting behaviors of the same samples after melt (or solution) crystallization. The neat PVDF and its composites (5–10 mg) were heated from 40 to 210 °C at a heating rate of 10 °C/min.

## 3. RESULTS AND DISCUSSION

**3.1. Comparison of Solution and Melt Crystallization in PVDF/GO Composites.** A comparative study on solution and melt crystallization in PVDF/GO composites was carried out first, aiming to evaluate the effect of solvents (DMF) and GO on the crystalline structure of PVDF. Figure 1a shows the (100) <sub>$\alpha$</sub>  at 17.6° in neat PVDF sample, and its intensity decreases and becomes invisible with the increase of the GO content, indicating that polar phase may form when GO is

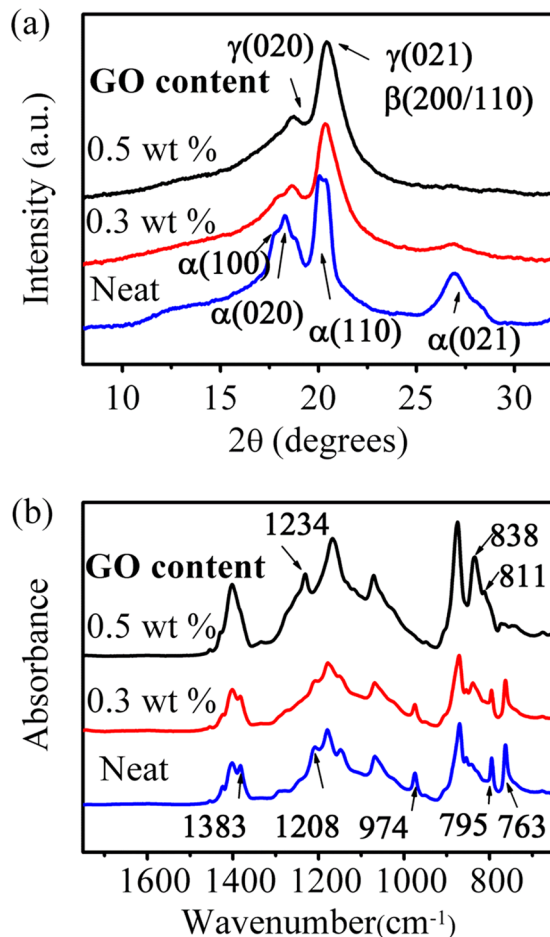


**Figure 1.** (a) WAXD profiles and (b) FTIR spectra of neat PVDF and PVDF/GO composites crystallized from DMF solution at 120 °C.

added into the PVDF solution in DMF. The reflection peak at  $2\theta = 20.4^\circ$  could be attributed to either  $(200/100)_\beta$  or  $(021)_\gamma$ , and it is also very close to  $(110)_\alpha$ .<sup>7,29,30</sup> Thus, to distinguish different crystalline structures in PVDF/GO composites crystallized from DMF solution, FTIR was utilized. Figure 1b is the FTIR spectra of the PVDF/GO composites crystallized from DMF solution at 120 °C. No absorption bands of DMF are seen<sup>31</sup> (C–N stretching mode at 1507  $\text{cm}^{-1}$ , N–C–H bending mode at 1388  $\text{cm}^{-1}$ , C–N asymmetric stretching at 1257  $\text{cm}^{-1}$ , C–N symmetric stretching at 866  $\text{cm}^{-1}$ , and the O=C–N stretching mode at 659  $\text{cm}^{-1}$ ), indicating complete removal of the solvent. For neat PVDF sample, the absorption bands that are assigned to characteristic peaks of the  $\alpha$  TGTG' conformation:<sup>32</sup> 763  $\text{cm}^{-1}$  (CF<sub>2</sub> bending and skeletal bending), 795  $\text{cm}^{-1}$  (CH<sub>2</sub> rocking), 974  $\text{cm}^{-1}$  (CH<sub>2</sub> twisting), 1208  $\text{cm}^{-1}$  (CF<sub>2</sub> stretching and CH<sub>2</sub> wagging), and 1383  $\text{cm}^{-1}$  (CH<sub>2</sub> deformation and CH<sub>2</sub> wagging) are shown in Figure 1b, further confirming the formation of almost pure  $\alpha$  phase during solution crystallization of PVDF without GO. For the PVDF/GO composites, intriguingly, the characteristic bands of  $\gamma$  phase emerge,<sup>33,34</sup> i.e., 811 (CH<sub>2</sub> rocking), 838 (CF<sub>2</sub> symmetrical stretching and C–C stretching), and 1234  $\text{cm}^{-1}$  (CF<sub>2</sub> asymmetrical stretching and rocking). The appearance of  $\gamma$  phase and no exclusive peak of  $\beta$  phase (1275  $\text{cm}^{-1}$ , CF<sub>2</sub> symmetrical and C–C asymmetrical stretching and skeletal deformation)<sup>32</sup> allow us to conclude that GO can only induce the polar  $\gamma$  phase rather than the  $\beta$  phase in PVDF solution in

DMF. Moreover, a higher GO content promotes the amount of  $\gamma$  phase formed in the DMF solution. One can see that the FTIR characteristic bands of the  $\gamma$  phase become stronger while those for the  $\alpha$  phase become weaker and eventually vanish at 0.5 wt % GO.

The melt crystallization of PVDF could be more interesting since melt processing is a facile fabrication method for specific PVDF/GO product. Figure 2 shows the WAXD and FTIR

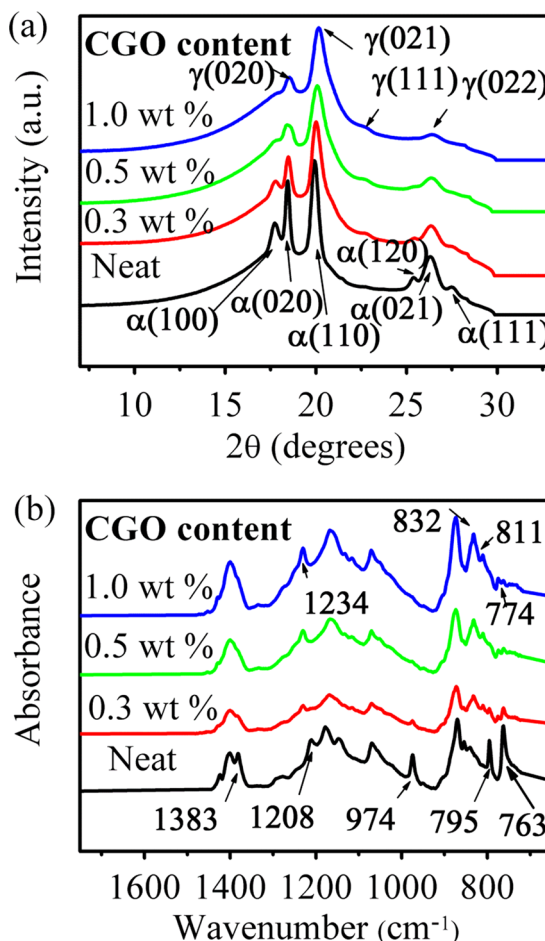


**Figure 2.** (a) WAXD profiles and (b) FTIR spectra of neat PVDF and PVDF/GO composites after melt crystallization at 160 °C for 80 min.

results of PVDF/GO composites isothermally crystallized from the melt at 160 °C. Unexpectedly, the results are quite different from the case of solution crystallization. Both neat PVDF and PVDF/GO composites show no trace of  $\gamma$  phase but  $\alpha$  phase. Namely, WAXD curves not only show the strong reflections of  $(100)_\alpha$ ,  $(020)_\alpha$ ,  $(110)_\alpha$  and  $(021)_\alpha$  like the case of neat PVDF crystallized from solution, but also some weak reflections of  $\alpha$  phase such as  $(120)_\alpha$  at 25.8° and  $(111)_\alpha$  at 27.5° (see Figure 2a). Furthermore, the FTIR spectrum also specifically shows characteristic bands of  $\alpha$  phase rather than those of  $\gamma$  (or  $\beta$ ) phase (see Figure 2b). These results confirm that almost pure  $\alpha$  phase is formed in the melt crystallization of PVDF regardless of the presence of GO. It should be noted that our results seem to be different from Yu's work,<sup>35</sup> in which more than one polymorph seem to form. Yu and co-workers used a slightly different method to fabricate PVDF/GO composites. Namely, the mixture of PVDF and GO sheets obtained from solution dispersion was dried on a hot plate at 120 °C, and then the

dried mixture was compressed into films at a relatively low temperature of 180 °C (lower than melting point of  $\gamma$  phase) under a high pressure. Our different results may infer that a different thermal history and processing procedure will affect the crystalline structure of PVDF, which should be investigated further in the future.

In order to investigate the effect of GO on the crystallization kinetics of  $\alpha$ -PVDF, time-resolved FTIR was utilized to probe the crystallization process by following the intensity and shape changes of the characteristic bands at 763, 795, 974, and 1208 cm<sup>-1</sup>. The time-resolved FTIR spectra of melt crystallization of PVDF with and without GO are shown in Figure 3. Intensity of the characteristic peaks for  $\alpha$  phase (e.g., 763 cm<sup>-1</sup>) apparently increases with the crystallization time. However, during the whole isothermal crystallization, we could not see any sign of the appearance of polar phases. Figure 3d shows the normalized (normalized with respect to the first curve of every peak) peak intensities at 763 cm<sup>-1</sup> as a function of crystallization time for neat PVDF and its composites. From this result, some useful parameters were extracted as listed in Table 1. The induction time of  $\alpha$  phase ( $t_i^\alpha$ ) is defined as the time at which the normalized intensity reaches 10%, and the half-crystallization time of  $\alpha$  phase ( $t_{1/2}^\alpha$ ) is defined as the time at which the normalized intensity reaches 50%. It can be clearly seen from Table 1 that  $t_i^\alpha$  and  $t_{1/2}^\alpha$  for the PVDF/GO composites are lower than those of neat PVDF ( $t_i^\alpha = 15$  min,  $t_{1/2}^\alpha = 22$  min). Moreover, as the GO content increases from 0.3 to 0.5 wt %,  $t_i^\alpha$  decreases from 13 to 10 min, and  $t_{1/2}^\alpha$  also decreases from 20 to 14.5 min. The decrease in  $t_i^\alpha$  and  $t_{1/2}^\alpha$  indicates that GO is an effective heterogeneous nucleating agent, which was also found in other polymers such as poly(L-lactide acid)<sup>36</sup> and isotactic polypropylene.<sup>28,37</sup> The strong heterogeneous nucleation may share the same mechanism, namely, PVDF chains are prone to interact with the surface of GO, leading to the low nucleation barrier of  $\alpha$ -PVDF. Although a direct evidence of this interaction can not be provided at the present stage, Zhao et al. reported recently that the TGTG' conformation of  $\alpha$  phase could be absorbed easily on the surface of carbon nanotubes due to the interaction between the H atom with partial positive charge in PVDF and C atom with  $\pi$  orbital in carbon nanotube.<sup>38</sup> Since both carbon nanotubes and GO have the same type of C atoms (i.e., graphene layers of sp<sup>2</sup>-bonded carbons), it is reasonable to argue that there are also interactions between GO and PVDF  $\alpha$ -TGTG' chains, triggering the crystallization process. As a result, both induction period and crystallization rate of  $\alpha$ -PVDF can be significantly affected by these interactions. The increased crystallization rate can be explained by more nucleation sites provided with the increase of GO loading in PVDF.

It is interesting to discuss why PVDF/GO composites exhibit  $\gamma$  phase from solution crystallization, but pure  $\alpha$  phase from melt crystallization. It seems that the dipole–dipole interaction between C–F and DMF plays a dominated role in inducing the TTT conformation for nucleation of  $\gamma$  phase. As PVDF is dissolved in its good solvent, DMF, the molecular chains spread out due to the strong interaction between the polar groups of DMF and the C–F dipole, creating some local order<sup>28</sup> with the formation of more extended trans conformation. This local trans conformation may facilitate the nucleation of a polar phase. This is also confirmed in other studies on polymorphism of PVDF crystallized in the mixture of its good solvent (DMF) and swelling agents (tetrahydrofuran (THF) or acetone).<sup>39,40</sup> At a relatively low temperature (50 or 40 °C), DMF leads to a

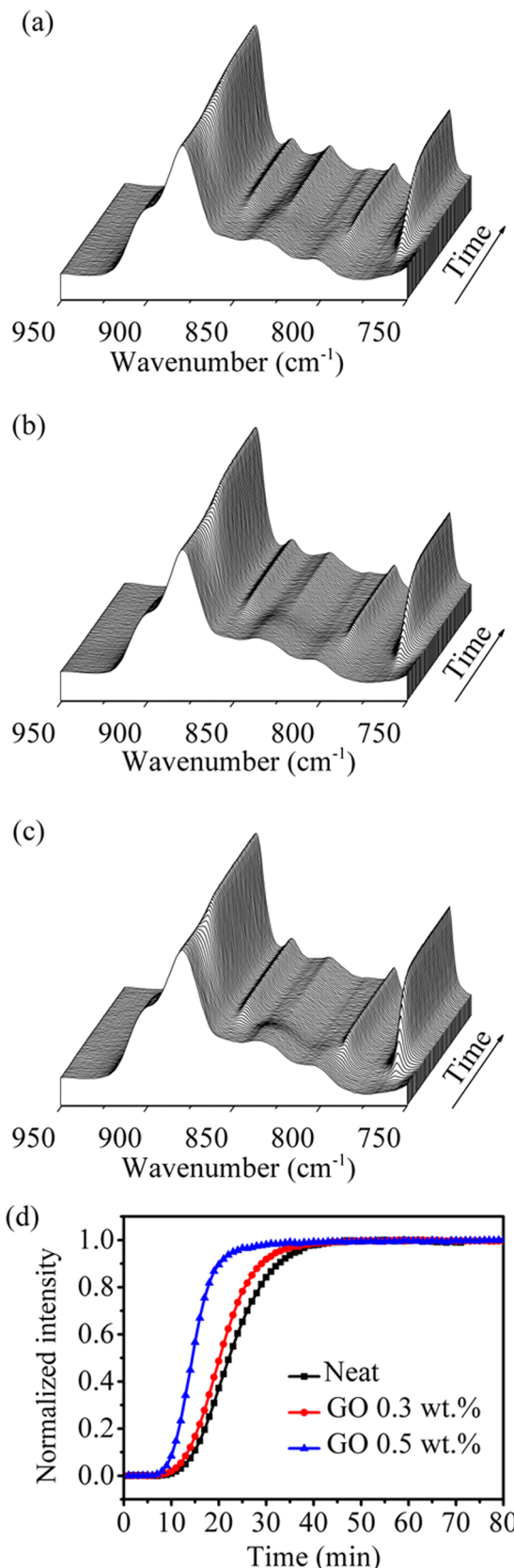


**Figure 3.** Time-resolved FTIR spectra in the range of 950–750 cm<sup>-1</sup> for (a) neat PVDF, (b) PVDF/GO (0.3 wt %) and (c) PVDF/GO (0.5 wt %) isothermally melt-crystallized at 160 °C. (d) Normalized peak intensity at 763 cm<sup>-1</sup> as a function of crystallization time for a, b, and c.

**Table 1.** Induction Time of  $\alpha$  Phase ( $t_i^\alpha$ ) and Half-Crystallization Time of  $\alpha$  Phase ( $t_{1/2}^\alpha$ ) of Neat PVDF and PVDF/GO Composites during Isothermal Melt-Crystallization

samples	induction time of $\alpha$ -crystal $t_i^\alpha$ (min)	half time of $\alpha$ crystallization $t_{1/2}^\alpha$ (min)
neat PVDF	15.0	22.2
PVDF/GO (0.3 wt %)	13.1	6.9
PVDF/GO (0.5 wt %)	10.1	14.5

pure polar phase, while THF or acetone generates mostly  $\alpha$  phase. The amount of polar phase increases with the DMF component. At higher temperature, however, this effect will diminish due to higher polymer chain mobility, reduced solvent polarity, and its lower ability to screen the  $\text{CF}_2$  group's electrostatic repulsion,<sup>26</sup> resulting in a exclusive formation of  $\alpha$  phase like our case of neat PVDF sample crystallized from solution at 120 °C.<sup>41</sup> More importantly, our results show that  $\gamma$  phase forms at high temperature from solution crystallization, but  $\alpha$  phase forms from melt crystallization in the presence of GO platelets. Naturally, we speculate that GO stabilizes the TTT conformation, rather than induces transition of TGTG' to TTG' conformation, which aids the nucleation of  $\gamma$  phase. This is probably because GO with  $\pi-\pi$  stacking structure prefers to absorb PVDF with a TTT conformation rather than a TGTG' conformation.<sup>38</sup> In summary, the  $\gamma$  phase formed from solution crystallization in PVDF/GO samples could be ascribed to the combined effect of the dipole–dipole interaction between C–F and DMF and the stabilizing effect of GO platelets.

**3.2. CGO-Induced  $\gamma$  Phase of PVDF.** Since polar phase of PVDF cannot be formed during melt crystallization of PVDF/GO composites due to the lack of strong local electric field-dipole interaction, we attempt to introduce stronger interactions, such as ion–dipole interaction, by a type of CGO platelet. As a cationic surfactant, CTAB is capable of self-aggregation as a micelle-like surfactant; a large number of hydrophilic ammonium ions may be located on the surface layer of self-aggregated micelles,<sup>42</sup> where the strong ion–dipole interaction between PVDF chains and micelles are expected to induce TTT conformation of PVDF. Figure 4a shows the WAXD profiles of PVDF/CGO composites melt-crystallized at 160 °C for 80 min. The characteristic peaks change apparently with the increase of CGO content. The reflection intensity of  $(100)_\alpha$  at  $2\theta = 17.6^\circ$  starts to decrease, and nearly vanishes at the CGO content of 1.0 wt %; the reflection of  $(110)_\alpha$  at  $2\theta = 20.1^\circ$  broadens and shifts to higher angle of  $2\theta=20.4^\circ$  upon addition of CGO, and a very weak but unique peak of  $(111)_\gamma$  at  $22.3^\circ$  is also observed. These results demonstrate that we successfully obtained a significant amount of polar phase and realized the manipulation of polymorphism in PVDF/GO composites. FTIR was applied to further investigate the crystalline structure existed in PVDF/CGO composites (Figure 4b). As shown in Figure 4b, with the increase of CGO content, the FTIR characteristics of  $\alpha$  phase (i.e., 763, 795, 974, 1208, and 1383  $\text{cm}^{-1}$ ) tend to disappear. At the same time, the intensities of  $\gamma$  phase bands at 832 and 1234  $\text{cm}^{-1}$  continue to increase. The relative amount of  $\gamma$  phase [ $F(\gamma)$ ] is calculated by eq 1 below:<sup>43,8</sup>

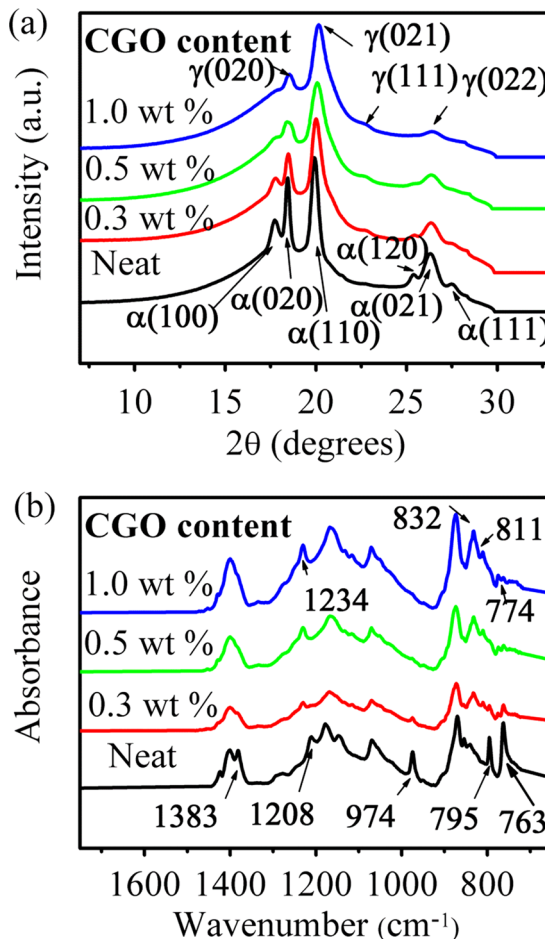


**Figure 4.** (a) WAXD profiles and (b) FTIR spectra of neat PVDF and PVDF/CGO composites after isothermal crystallization at 160 °C for 80 min.

$$F(\gamma) = \frac{X_\gamma}{X_\alpha + X_\gamma} = \frac{A_\gamma}{(K_\gamma/K_\alpha) + A_\gamma} \quad (1)$$

where  $A_\alpha$  and  $A_\gamma$  represent the absorbencies of  $\alpha$  and  $\gamma$  phase at 766 and 832  $\text{cm}^{-1}$ , respectively,  $K_\alpha$  and  $K_\gamma$  are the corresponding absorption coefficients, and  $X_\alpha$  and  $X_\gamma$  are the crystallinities of  $\alpha$  and  $\gamma$  phase. The value of  $K_\alpha$  is 0.365  $\mu\text{m}^{-1}$  and  $K_\gamma$  is 0.150  $\mu\text{m}^{-1}$ .<sup>43</sup> As listed in Table 2, with increasing of

**Table 2.** Relative Amount of  $\gamma$  Phase in PVDF/CGO Composites with Different CGO Contents after Melt Crystallization at 160 °C for 80 min

CGO content (wt %)	0.3	0.5	1.0
percentage of $\gamma$ phase (%)	78.8	91.0	95.8

CGO content from 0.3 to 0.5 wt %, the relative amount of  $\gamma$  phase rises from 78.8% to 91.0%. As CGO content is 1.0 wt %, the percentage of  $\gamma$  phase reaches up to 95.8%, i.e., almost pure  $\gamma$  phase has been achieved in PVDF/CGO composite from melt crystallization by addition of a small amount of CTAB (0.25%). Since pristine GOs are prone to induce  $\alpha$  phase (see Figure 3), it seems that the addition of CTAB could transfer the nonpolar interface of pristine GO into the polar interface of CGO, facilitating the nucleation of polar phase of PVDF. Ordered parallel stripes arranged in a head-to-head configuration with approximately twice the length of a surfactant

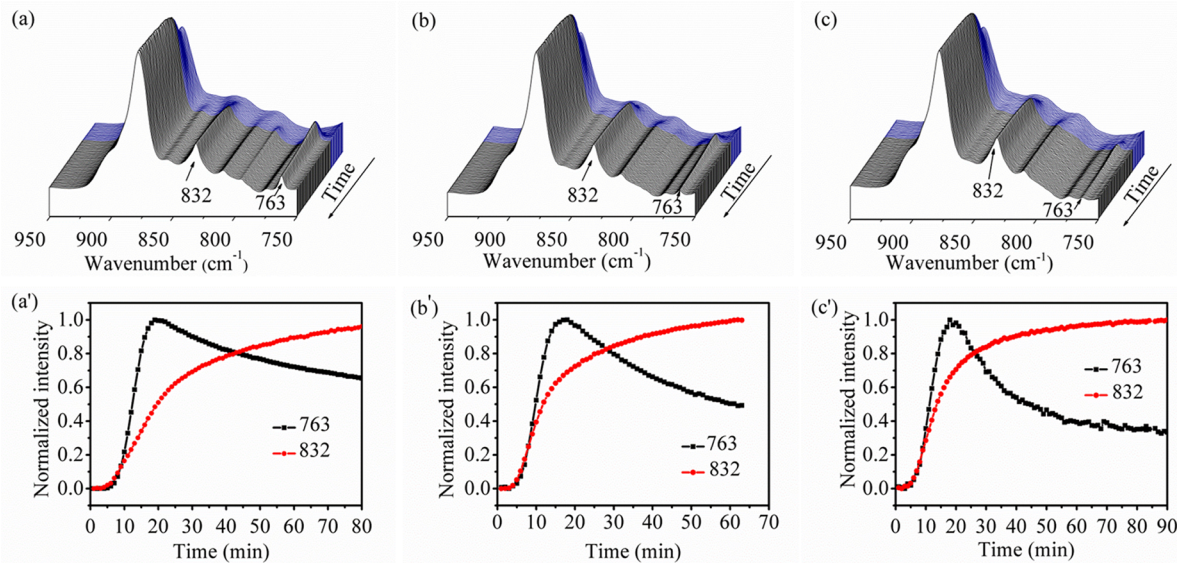


**Figure 5.** (a–c) Time-resolved FTIR spectra and (a'–c') normalized peak intensities at 763 cm<sup>-1</sup> and 832 cm<sup>-1</sup> during isothermal crystallization (160 °C) of PVDF/CGO composites with different CGO contents: (a,a'), 0.3 wt %; (b,b'), 0.5 wt %; (c,c'), 1.0 wt %.

molecule were verified by some direct observations by scanning tunneling microscope,<sup>44</sup> and later the molecular dynamics simulations showed continuous hemicylinders structures.<sup>45</sup> Namely, the tail groups of CTAB can absorb strongly to the graphite surface in tail-to-tail packing interactions caused by the alkyl tail in registry with the substrate lattice, while the head groups of the CTAB molecules expose outward.<sup>46</sup> The ionic head groups would attract the C–F dipole, thus inducing more extended TTTGTTTG' conformation and promoting the nucleation of  $\gamma$  phase. When the CGO content is low, the PVDF chains in the vicinity of GO platelets tend to be long trans conformation because of the ion–dipole interactions, and subsequently nucleates into  $\gamma$  phase. However, the  $\alpha$  phase crystallization occurs far away from the CGO platelets, thus a mixture of  $\gamma$  and  $\alpha$  phase appears. When CGO content is high, an exclusive  $\gamma$  phase forms due to sufficient CGO surface to induce T<sub>3</sub>GT<sub>3</sub>G' conformation for nearly all PVDF chains.

Note that the characteristic bands for  $\gamma$  phase formed from solution and melt crystallization have subtle differences. The bands of 774 and 832 cm<sup>-1</sup>, which refer to ordered T<sub>3</sub>GT<sub>3</sub>G' conformation, are observed in melt-crystallized samples, whereas the samples crystallized from solution only show the band of 838 cm<sup>-1</sup>. Such a difference may be due to the different length of TTT conformation formed in solution and melt. For solution-cast film,  $\gamma$  phase contains some long trans sequences as a kind of defect within the basic T<sub>3</sub>GT<sub>3</sub>G' conformation, therefore the band characteristic representing  $\gamma$  phase (838 cm<sup>-1</sup>) would tend to approach the long trans sequence band of 840 cm<sup>-1</sup>; meanwhile, the weak characteristic band of ordered T<sub>3</sub>GT<sub>3</sub>G' (774 cm<sup>-1</sup>) may not be detected. This phenomenon was also reported in the PVDF samples annealed close to the melting point, leading to disorder to order transition of molecular conformation.<sup>33</sup>

The formation of crystalline polymorphism in the melt-recrystallized samples was studied by time-resolved FTIR, and results are shown in Figure 5. Generally, the crystal sensitive bands for  $\gamma$  and  $\alpha$  phases appear and subsequently increase in their intensities during isothermal crystallization. To reveal the growth of  $\alpha$  phase and  $\gamma$  phase in details, the intensities of 763 cm<sup>-1</sup> band for the  $\alpha$  phase and 832 cm<sup>-1</sup> band for the  $\gamma$  phase

are extracted. The normalized intensity of the two bands as a function of crystallization time is given in Figure 5a'–c'. It is interesting to see that the crystallization process can be divided into two stages. In the first stage, the intensities of both 763 and 832 cm<sup>-1</sup> bands increase rapidly. Thereafter, the 763 cm<sup>-1</sup> band decreases accompanying with the increase of 832 cm<sup>-1</sup> in the second stage.

Table 3 further illustrates ultimate absolute intensities of 763 cm<sup>-1</sup> and 832 cm<sup>-1</sup> after extracting the influence of thickness at

**Table 3.** Ultimate Absolute Intensities of 763 and 832 cm<sup>-1</sup> Bands at Different Stages during the Melt Crystallization of PVDF with Various Concentrations of CGO after Extracting the Influence of Thickness

sample	the first stage		the second stage	
	763	832	763	832
PVDF/CGO (0.3 wt %)	0.1491	0.1126	0.1157	0.1880
PVDF/CGO (0.5 wt %)	0.0774	0.1580	0.0415	0.2108
PVDF/CGO (1.0 wt %)	0.0496	0.1754	0.0216	0.2426

the two stages (see details in Figure S3). In the first stage, the ultimate absolute intensity of 763 cm<sup>-1</sup> reduces while the intensity of 832 cm<sup>-1</sup> increases with the increase of CGO content, thus demonstrating again that CGO facilitates the  $\gamma$  phase formation. In the second stage, it is elucidated from ultimately absolute intensity decrease of 763 cm<sup>-1</sup> band and increase of 832 cm<sup>-1</sup> that a transition from  $\alpha$  to  $\gamma$  phase occurs during isothermal melt crystallization. Takahashi<sup>48</sup> proposed a mechanism in which the segmental flip-flop motion led to the transformation from TGTG' to T<sub>3</sub>GT<sub>3</sub>G' conformation, while inversion motion changed the molecular packing from the antiparallel structure to the parallel structure. Therefore, the  $\alpha$ – $\gamma$  solid transition took place. The  $\alpha$ – $\gamma$  transition is also observed when the  $\alpha$  phase is annealed in the vicinity of its melting point;<sup>48,49</sup> a surfactant-aided transition was even reported by Prest and Luca during the process in which an  $\alpha$  phase PVDF coated by a copolymer-type surfactant was slowly heated to a temperature near its melting point.<sup>48</sup> It was proposed that the copolymer surfactant interfered with the

diffusion of molecules during the melting process, which seems to originate from dipole–dipole interactions, which is similar to our results found in electrospun PVDF/PAN blends.<sup>18</sup> In our case, we attribute the preferential nucleation of  $\gamma$  phase to the ion–dipole interaction between polymer chain and CTAB micelles. When assuming that their molecular absorption coefficients at 811 and 795  $\text{cm}^{-1}$  are the same, the linear relationship between 796 and 811  $\text{cm}^{-1}$  bands could reflect the details of  $\alpha$ – $\gamma$  transition, since the FTIR bands at 796 and 811  $\text{cm}^{-1}$  are all assigned to the same mode ( $\text{CH}_2$  rocking mode) of  $\alpha$  phase and  $\gamma$  phase, respectively.<sup>50</sup> In the case of a  $\gamma$  phase deriving completely from solid state transformation of  $\alpha$  phase, the process should be first-order kinetics; by contrast, in the case of melt crystallization of  $\gamma$  phase, the rate of  $\gamma$  phase formation would be independent of  $\alpha$  phase concentration (i.e., zero-order kinetics). Thereby, the slope of  $-1$  suggests that there is only an  $\alpha$ – $\gamma$  transition in solid state. When the slope is larger than  $-1$ , it means that a direct nucleation and crystallization of  $\gamma$  phase occurs except for the solid  $\alpha$ – $\gamma$  transition. As shown in Figure 6, a direct crystallization of  $\gamma$

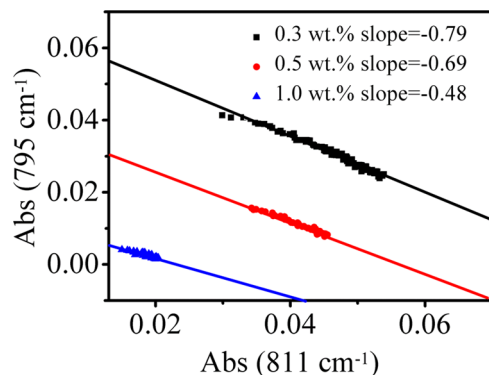


**Figure 6.** Relationship between the increase of absorbance at 811  $\text{cm}^{-1}$  and the decrease of absorbance at 795  $\text{cm}^{-1}$  for PVDF/CGO composites with different CGO contents.

phase other than  $\alpha$ – $\gamma$  transition also exists during the second stage since the slopes for all PVDF/CGO samples are larger than  $-1$ . Moreover, the increase of slope with the CGO content reveals that the CGO is favorable for the formation of melt-crystallized  $\gamma$  phase.

On the basis of Figure 5(a’–c’), we can also investigate the crystallization kinetics of  $\alpha$  phase and  $\gamma$  phase, respectively. The induction time and half-crystallization time for each phase formed in PVDF/CGO composites are summarized in Table 4. It can be clearly seen that the introduction of ion–dipole interaction also has a more favorable effect on nucleation of  $\alpha$  phase in the first stage than that of GO. The  $t_i^\alpha$  and  $t_{1/2}^\alpha$  of

PVDF/CGO composites are shorter than that of neat PVDF as well as PVDF/GO composites. For instance, the  $t_i^\alpha$  and  $t_{1/2}^\alpha$  of PVDF/GO (0.3 wt %) composites are 13.1 and 20.0 min, respectively (see Table 1), whereas those of PVDF/CGO (0.3 wt %) are 8.5 and 12.2 min, respectively (see Table 4). For  $\gamma$  phase, as the CGO content increases from 0.3 to 0.5 wt %, the induction time of  $\gamma$  phase ( $t_i^\gamma$ ) decreases from 8.1 to 5.8 min and the half-crystallization time of  $\gamma$  phase ( $t_{1/2}^\gamma$ ) rises from 19.7 to 11.7 min. In addition, the  $t_i^\alpha$  in all PVDF/CGO composites is shorter than that of  $\alpha$  phase also verifies that nucleation of  $\gamma$  phase is kinetically favorable in the presence of CTAB because of the effect of ion–dipole interaction on the formation of polar phase mentioned above. It is noted that when CGO content is 1.0 wt %, the  $t_i^\gamma$  and  $t_{1/2}^\gamma$  (7.0 and 13.8 min) are slightly lower than those of the samples with the CGO content of 0.3 and 0.5 wt % (see Table 4). This slower crystallization rate may be due to the slightly confined effect of nanofillers on crystallization as observed in some nanocomposites.<sup>51,52</sup>

Melting behavior of melt-crystallized PVDF/CG composites is also investigated by DSC and time-resolved FTIR. For comparison, Figure 7a show DSC melting traces of neat PVDF and PVDF/GO composites. The melting peak around 175  $^{\circ}\text{C}$  is attributed to  $\alpha$  phase since only  $\alpha$  phase forms in these systems (see Figure 2). As shown in Figure 7b, three endothermic peaks can be identified in the DSC curves for the PVDF/CGO (0.3 wt %) composite, i.e., the lowest peak around 175  $^{\circ}\text{C}$ , the middle peak around 182  $^{\circ}\text{C}$ , and the highest one around 192  $^{\circ}\text{C}$ . The three melting peaks of the PVDF isothermally crystallized at a high temperature have been reported by some researchers.<sup>47–50,53,54</sup> They confirmed that with enough time for isothermal crystallization or annealing, an  $\alpha$ – $\gamma$  solid-state phase transformation would take place, with a 8–10  $^{\circ}\text{C}$  higher melting peak for the  $\gamma$ -phase emerging.

In our case, the lowest melting peak can be assigned to the melting of  $\alpha$  phase easily based on comparison of the results of PVDF/CGO and PVDF/GO system. To clarify the other two higher melting peaks, Figure 8 gives the selective time-resolved FTIR spectra of PVDF/CGO composite during heating. The intensities for the characteristic bands of  $\gamma$  and  $\alpha$  phases decrease due to melting, and normalized intensity of time-resolved FTIR in melting process reveals that the peak of 763  $\text{cm}^{-1}$  of  $\alpha$  phase disappears at  $\sim$ 176  $^{\circ}\text{C}$  while 832  $\text{cm}^{-1}$  of  $\gamma$  phase vanishes at  $\sim$ 192  $^{\circ}\text{C}$  (see Figure 9 and other data in Figure S3). No phase transition detected during heating suggests that the two higher melting peaks are attributed to crystals formed in the isothermal melt crystallization rather than the heating process of DSC. As verified by the results of Figures 5 and 6, there are two type of  $\gamma$  crystallites (i.e., from direct melt crystallization and solid–solid transition) formed in isothermal melt crystallization, which should be related to the

**Table 4. Induction Time ( $t_i$ ) and Half-Crystallization Time ( $t_{1/2}$ ) of Neat PVDF and PVDF Composites<sup>a</sup>**

samples	induction time of $\alpha$ crystallization $t_i^\alpha$ (min)	induction time of $\gamma$ crystallization $t_i^\gamma$ (min)	half time of $\alpha$ crystallization $t_{1/2}^\alpha$ (min)	half time of $\gamma$ crystallization $t_{1/2}^\gamma$ (min)
PVDF/CGO (0.3 wt %)	8.5	8.1	12.2	19.7
PVDF/CGO (0.5 wt %)	6.5	5.8	9.7	11.7
PVDF/CGO (1.0 wt %)	7.4	7.0	10.9	13.8

<sup>a</sup>The definitions of  $t_i$  and  $t_{1/2}$  are the same as in Table 1, only difference is that  $t_{1/2}^\alpha$  indicates the time at which the relative crystallinity of  $\alpha$  phase reaches 50% in the first stage.

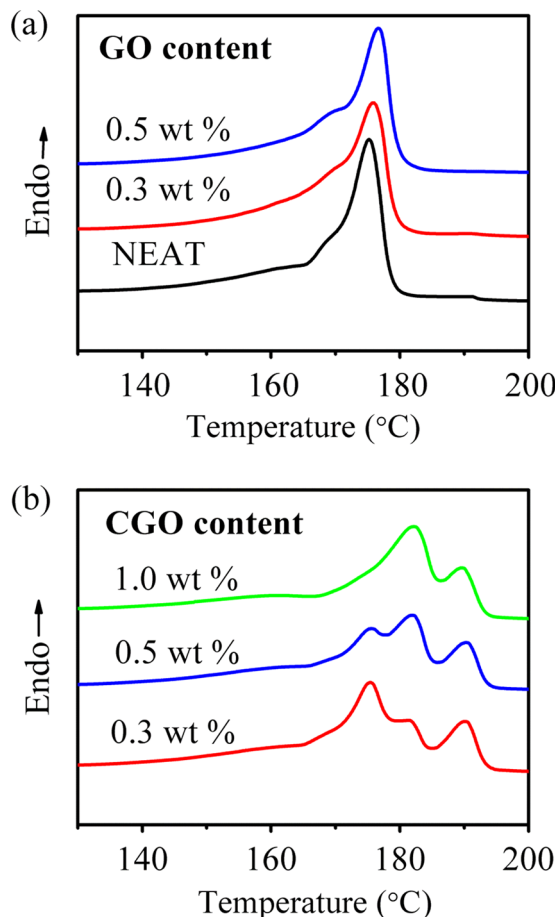


**Figure 7.** DSC melting curves of (a) neat PVDF, PVDF/GO, and (b) PVDF/CGO composites after isothermal crystallization at 160 °C for 80 min.

two melting peaks. The area of middle peak increases with the concentration of CGO while the area of the highest peak is nearly unchanged, inferring that the middle peak is the melting point of the  $\gamma$  crystallites from direct melt crystallization since the amount of melt-crystallized  $\gamma$  phase can be promoted by the content of CGO, as confirmed by Table 3. The highest one should be assigned to the melting of the  $\gamma$  crystallites from the  $\alpha$ - $\gamma$  phase transition during isothermal melt crystallization. The  $T_m$  of  $\gamma$  phase formed from solid-solid transition is about 10 °C higher than that directly melt-crystallized  $\gamma$  phase. This is probably because the solid-solid transition takes place in an annealing process and the crystals formed are supposed to be more ordered than those melt-crystallized directly, which is also reported in annealed PVDF previously.<sup>9,53,54</sup>

#### 4. CONCLUSIONS

We systematically investigated the melt crystallization and polymorphism of PVDF/GO composites with and without ionic surfactant. It is shown that the interaction between GO and PVDF is too weak to induce any polar phase during melt crystallization, but is favorable for stabilizing TTT conformation to nucleation of  $\gamma$  phase in the presence of a polar solvent (DMF). Although only  $\alpha$  phase forms in PVDF/GO composites during the isothermal melt crystallization, the manipulation on the polymorphism in PVDF/GO composites was achieved by introducing strong ion-dipole interactions through coating of an ionic surfactant (CTAB) on the GO

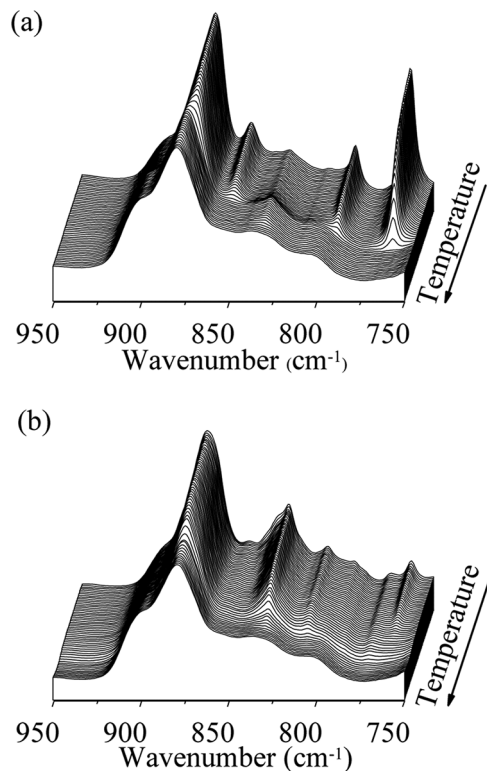


**Figure 8.** Time-resolved FTIR spectra in the range of 950–750 cm<sup>-1</sup> of (a) PVDF/GO (0.5 wt %) and (b) PVDF/CGO (0.5 wt %) in the melting process. The heating rate is 2 °C/min.

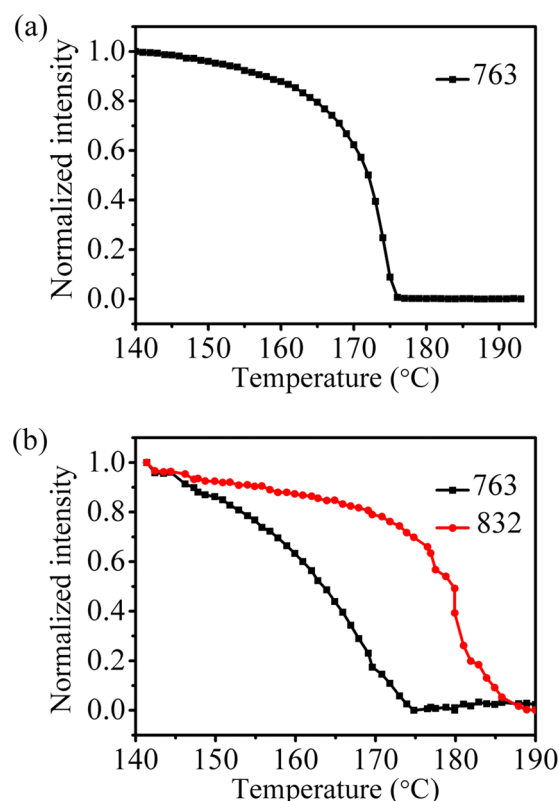


**Figure 9.** Normalized intensities at 763 cm<sup>-1</sup> and 832 cm<sup>-1</sup> as a function of temperature for (a) PVDF/GO (0.5 wt %) and (b) PVDF/CGO (0.5 wt %). The heating rate is 2 °C/min.

surfaces. Nearly pure  $\gamma$  crystals were obtained after melt crystallization. Time-resolved FTIR further revealed two stages of crystallization existing during the formation of  $\gamma$  phase in PVDF melt. Namely, the growth of  $\gamma$  and  $\alpha$  phases simultaneously in the first stage and the second stage comprises a solid–solid transition from  $\alpha$  to  $\gamma$ . DSC results indicated that the  $T_m$  of  $\gamma$  phase formed from solid–solid transition is about 10 °C higher than that directly crystallized from the melt due to highly ordered structure via annealing.

## ■ ASSOCIATED CONTENT

### S Supporting Information

FTIR spectra and TGA curves of CTAB, GO, and CGO. TEM images of PVDF/GO (0.5 wt %) and PVDF/CGO (1.0 wt %) composites. The method of internal correction for extracting thickness influence. Normalized peak intensities at 763 cm<sup>-1</sup> and 832 cm<sup>-1</sup> as a function of melting temperature for PVDF/CGO (0.3 wt %) composite and PVDF/CGO (1.0 wt %) composite. This material is available free of charge via the Internet at <http://pubs.acs.org>.

## ■ AUTHOR INFORMATION

### Corresponding Author

\*Tel.: +86-28-8540-6866; Fax: +86-28-8540-6866. E-mail addresses: zml@scu.edu.cn (Z.-M.L.); ganji.zhong@scu.edu.cn (G.-J.Z.).

### Notes

The authors declare no competing financial interest.

## ■ ACKNOWLEDGMENTS

The authors acknowledge the support from the National Natural Science Foundation of China (Grant Nos. 51120135002, 51121001, and 51203104), and the startup fund of Sichuan University (Grant No. 2011SCU11072). We also would like to express sincere thanks to the National Synchrotron Radiation Laboratory (NSRL), Shanghai, for assistance with 2D WAXD measurements.

## ■ REFERENCES

- (1) Takahashi, Y.; Matsubara, Y.; Tadokoro, H. *Macromolecules* **1983**, *16*, 1588–1592.
- (2) Tadokoro, Y.; Tadokoro, H. *Macromolecules* **1980**, *13*, 1317–1318.
- (3) Naegle, D.; Yoon, D. Y.; Broadhurst, M. G. *Macromolecules* **1978**, *11*, 1297–1298.
- (4) Weinhold, S.; Bachmann, M. A.; Litt, M. H.; Lando, J. B. *Macromolecules* **1982**, *15*, 1631–1633.
- (5) Pfister, G.; Abkowitz, M.; Crystal, R. G. *J. Appl. Phys.* **1973**, *44*, 2064–2070.
- (6) Kochervinski, V. V. *Crystallog. Rep.* **2003**, *48*, 649–675.
- (7) Tashiro, K.; Takano, K.; Kobayashi, M.; Chatani, Y.; Tadokoro, H. *Polym. Bull.* **1983**, *10*, 464–469.
- (8) Lopes, A. C.; Costa, C. M.; Tavares, C. J.; Neves, I. C.; Mendez, S. L. *J. Phys. Chem. C* **2011**, *115*, 18076–18082.
- (9) Miyazaki, T.; Takeda, Y.; Akasaka, M.; Sakai, M.; Hoshiko, A. *Macromolecules* **2008**, *41*, 2749–2753.
- (10) Lovinger, A. J. *Macromolecules* **1981**, *14*, 322–325.
- (11) Minami, Y.; Nakamura, K.; Takahashi, Y.; Furukawa, T. *13th International Symposium on Electrets*, 2008. ISE 13 pp1. DOI: 10.1109/ISE.2008.4814059
- (12) Ince-Gunduz, B. S.; Alpern, R.; Amare, D.; Crawford, J.; Dolan, B.; Jones, S.; Kobylar, R.; Reveley, M.; Cebe, P. *Polymer* **2010**, *51*, 1485–1494.
- (13) Manna, S.; Nandi, A. K. *J. Phys. Chem. C* **2007**, *111*, 14670–14680.
- (14) Xing, C. Y.; Zhao, L. Y.; You, J. C.; Dong, W. Y.; Cao, X. J.; Li, Y. *J. J. Phys. Chem. B* **2012**, *116*, 8312–8320.
- (15) Yousefi, A. A. *Iran. Polym. J.* **2011**, *20* (2), 109–121.
- (16) Gao, Q.; Scheinbeim, J. I. *Macromolecules* **2000**, *33*, 7564–7572.
- (17) Li, Y. J.; Shimizu, H.; Furumichi, T.; Takahashi, Y.; Furukawa, T. *J. Polym. Sci. Polym. Phys.* **2007**, *45*, 2707–2720.
- (18) Zhong, G. J.; Zhang, L. F.; Su, R.; Wang, K.; Fong, H.; Zhu, L. *Polymer* **2011**, *52* (10), 2228–2237.
- (19) Stankovich, S.; Dikin, D. A.; Dommett, G. H. B.; Kohlhaas, K. M.; Zimney, E. J.; Stach, E. A.; Piner, R. D.; Nguyen, S. T.; Ruoff, R. S. *Nature* **2006**, *442* (7100), 282–286.
- (20) Yu, J. H.; Huang, X. Y.; Wu, C.; Jiang, P. K. *IEEE Trans. Dielect. Electr. Insul.* **2011**, *18* (2), 478–484.
- (21) Li, Y. C.; Tjong, S. C.; Li, R. K. Y. *Synthet. Met.* **2010**, *160*, 1912–1919.
- (22) Eswaraiah, V.; Sankaranarayanan, V.; Ramaprabhu, S. *Macromol. Mater. Eng.* **2011**, *296* (10), 894–898.
- (23) Layek, R. K.; Samanta, S.; Chatterjee, D. P.; Nandi, A. K. *Polymer* **2010**, *51* (11), 5846–5855.
- (24) Achaby, M. E.; Arrakhiz, F. Z.; Vaudreuil, S.; Essassi, E. M.; Qaiss, A. *Appl. Surf. Sci.* **2012**, *258* (19), 7668–7677.
- (25) Zhang, Y. Y.; Jiang, S. L.; Yu, Y.; Zeng, Y. K.; Zhang, G. Z.; Zhang, Q. F.; He, J. G. *J. Appl. Polym. Sci.* **2012**, *125* (1), 314–319.
- (26) Salimi, A.; Yousefi, A. A. *J. Polym. Sci., Part B: Polym. Phys.* **2003**, *42*, 3487–3495.
- (27) Benz, M.; Euler, W. B.; Gregory, O. J. *Macromolecules* **2002**, *35*, 2682–2688.
- (28) Xu, J. Z.; Chen, C.; Wang, Y.; Tang, H.; Li, Z. M.; Hsiao, B. S. *Macromolecules* **2011**, *44*, 2808–2818.
- (29) Hattori, T.; Masamichi, H.; Ohigashi, H. *Polymer* **1995**, *37* (1), 85–91.
- (30) Matsushige, K.; Nagata, K.; Takemura, T. *Jpn. J. Appl. Phys.* **1978**, *17*, 467–472.
- (31) Jacob, M. M. E.; Arof, A. K. *Electrochim. Acta* **2000**, *45*, 1701–1706.
- (32) Kobayashi, M.; Tashiro, K.; Tadokoro, H. *Macromolecules* **1975**, *8* (2), 158–171.
- (33) Tashiro, K.; Kobayashi, M.; Tadokoro, H. *Macromolecules* **1981**, *14*, 1757–1764.
- (34) Bachmann, M. A.; Gordon, W. L. *J. Appl. Phys.* **1979**, *50*, 6106–6113.
- (35) Yu, J. H.; Jiang, P. K.; Wu, C.; Wang, L. C.; Wu, X. F. *Polym. Compos.* **2011**, *32* (10), 1483–1491.
- (36) Xu, J. Z.; Chen, T.; Yang, C. L.; Li, Z. M.; Mao, Y. M.; Zeng, B. Q.; Hsiao, B. S. *Macromolecules* **2010**, *43*, 5000–5008.
- (37) Xu, J. Z.; Liang, Y. Y.; Zhong, G. J.; Li, H. L.; Chen, C.; Li, L. B.; Li, Z. M. *J. Phys. Chem. Lett.* **2012**, *3* (4), 530–535.
- (38) Yu, S. S.; Zheng, W. T.; Yu, W. X.; Zhang, Y. J.; Jiang, Q.; Zhao, Z. D. *Macromolecules* **2009**, *42*, 8870–8874.
- (39) Ma, W. Z.; Zhang, J.; Chen, S. J.; Wang, X. L. *J. Macromol. Sci. B* **2008**, *47*, 434–459.
- (40) Zhao, X. J.; Cheng, J.; Chen, S. J.; Wang, X. L. *J. Polym. Sci., Part B: Polym. Phys.* **2010**, *48*, 575–582.
- (41) Gregorio, R.; Borges, D. S. *Polymer* **2008**, *49*, 4009–4016.
- (42) Kuperkar, K.; Abezgauz, L.; Prasad, K.; Bahadur, P. *J. Surfactants Deterg.* **2010**, *13*, 293.
- (43) Benz, M.; William, B. E. *J. Appl. Polym. Sci.* **2003**, *89*, 1093–1100.
- (44) Xu, S. L.; Wang, C.; Zeng, Q. D.; Wu, P.; Wang, Z. G.; Yan, H. K.; Bai, C. L. *Langmuir* **2002**, *18*, 657–660.
- (45) Srinivas, G.; Nielsen, S. O.; Moore, P. B.; Klein, M. L. *J. Am. Chem. Soc.* **2006**, *128*, 848–853.
- (46) Kiraly, Z.; Findenegg, G. H. *J. Phys. Chem. B* **1998**, *102*, 1203–1211.
- (47) Takahashi, Y.; Matsubara, Y.; Tadokoro, H. *Macromolecules* **1982**, *15*, 334–338.
- (48) Prest, W. M.; Luca, D. *J. Appl. Phys.* **1978**, *49* (10), 5042–5051.
- (49) Gregorio, R.; Capitao, R. C. J. *Mater. Sci.* **2000**, *35*, 299–306.

- (50) Zhang, G. Z.; Kitamura, T.; Yoshida, H.; Kawai, T. *J. Therm. Anal. Calorim.* **2002**, *69*, 939–948.
- (51) Wang, H. P.; Keum, J. K.; Hiltner, A.; Baer, E. *Macromolecules* **2009**, *42* (18), 7055–7066.
- (52) Xu, D. H.; Wang, Z. G. *Polymer* **2008**, *49*, 330–338.
- (53) Prest, W. M.; Luca, D. J. *J. Appl. Phys.* **1975**, *46* (10), 4136–4143.
- (54) Silva, M. P.; Sencadas, V.; Botelho, G.; Machado, A. V.; Rolo, A. G.; Rocha, J. G.; Mendez, S. L. *Mater. Chem. Phys.* **2010**, *122*, 87–92.